

Contributed Paper

The role of the diffuse ionized gas in metallicity calibrations

N. Vale Asari^{1,2}

¹*Depto. de Física – CFM – UFSC, Florianópolis, SC, Brazil*

²*Royal Society–Newton Advanced Fellowship*

Abstract. Estimates of gas-phase abundances based on strong-line methods have been calibrated for H II regions. Those methods ignore any contribution from the diffuse ionized gas (DIG), which shows enhanced collisional-to-recombination line ratios in comparison to H II regions of the same metallicity. Applying strong line methods whilst ignoring the role of the DIG thus systematically overestimates metallicities. Using integral field spectroscopy data, we show how to correct for the DIG contribution and how it biases the mass–metallicity–star formation rate relation.

Key words: galaxies: abundances — galaxies: ISM

1. Introduction

The diffuse ionized gas (DIG) is a warm (10^4 K), low-density (10^{-1} cm $^{-3}$) gas phase in the interstellar medium. The DIG was first detected outwith the plane of the Milky Way, and later on as extraplanar emission in other galaxies, in interarm regions, and in bulges of galaxies (e.g. Hoyle & Ellis, 1963; Dettmar, 1990; Gomes et al., 2016). Apart from their lower densities compared to H II regions, the DIG has been found to have higher electronic temperatures and enhanced collisional-to-recombination line ratios, such as [N II] λ 6584/H α , [S II] λ 6716/H α , and for some objects [O III] λ 5007/H β . For a thorough review of the DIG, see Haffner et al. (2009) and references therein.

The enhanced collisional-to-recombination line ratios imply that the DIG must be ionized by a source that is harder than OB stars. Several sources have been proposed, such as shocks from supernova winds, turbulent dissipation, photoelectric heating by grains, leakage of photons from H II regions, and hot low mass evolved stars (HOLMES, Stasińska et al., 2008; Flores-Fajardo et al., 2011).

Regardless of its ionization mechanism, the presence of the DIG biases commonly used estimates of gas-phase abundances. Consider a hypothetical galaxy with a single value of oxygen abundance (O/H). The presence of the DIG would enhance [N II]/H α . If we were to obtain O/H from the [N II]/H α index using a strong line method, which has been calibrated for H II regions, we would wrongly conclude this galaxy has a higher O/H than it really does. The larger the contribution of the DIG, the more O/H is overestimated when using strong-line methods. We investigate the effect of the DIG on integrated values of O/H based on integral field spectroscopy (IFS) from Mapping Nearby Galaxies at

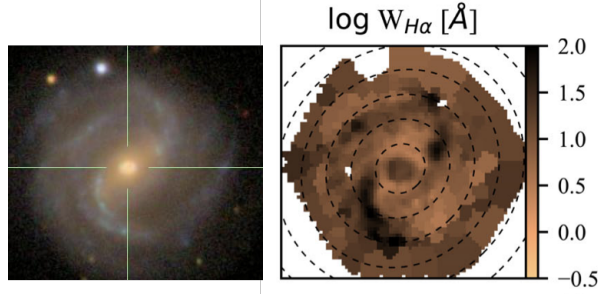


Figure 1. Right: optical SDSS image of galaxy NGC 0776. Left: map of $H\alpha$ equivalent width of the same galaxy based on CALIFA observations. High values of $W_{H\alpha}$ trace the spiral arms, denoting its usefulness in separating emission dominated by H II regions from emission dominated by the DIG in the bulge and interarm regions. (Figure adapted from figure 1 by Lacerda et al., 2018.)

APO (MaNGA, Blanton et al., 2017). Vale Asari et al. (2019), hereafter VA19, detail the sample selection and data processing. The next sections summarize their main findings.

2. Identifying the DIG

Three main ways have been used to identify regions dominated by the DIG in IFS data: using a threshold for (1) the $H\alpha$ surface brightness, (2) a collisional-to-recombination line ratio such as $[S II]/H\alpha$, and (3) the $H\alpha$ equivalent width ($W_{H\alpha}$). A cut in $H\alpha$ surface brightness (e.g. Zhang et al., 2017) hinges on the fact that the DIG is less dense than H II regions. This criterion is not appropriate for central parts of galaxies, as argued by Lacerda et al. (2018), since the projected surface brightness would be enhanced. $W_{H\alpha}$, being an intensive quantity, remains small and can correctly identify DIG-dominated regions even in bulges. A cut in $[S II]/H\alpha$ (e.g. Kaplan et al., 2016) would be inappropriate here, since we aim to quantify the effect of the DIG on the very same emission lines. We thus find $W_{H\alpha}$ to be the best physically motivated criterion for our dataset.

Figure 1 shows an optical image of NGC 0776 and a map of its observed $W_{H\alpha}$ obtained from the Calar Alto Legacy Integral Field Area Survey (CALIFA; Sánchez et al., 2016). High- $W_{H\alpha}$ spaxels trace the spiral arms, whereas small- $W_{H\alpha}$ spaxels are in the interarm regions dominated by the DIG. The reasoning behind using $W_{H\alpha}$ is that nebulae ionized by H II regions have large values of $W_{H\alpha}$, whereas those ionized by HOLMES (see figure 2 by Cid Fernandes et al., 2011) or e.g. by hard photons leaking from H II regions would have small $W_{H\alpha}$ values. Implicit in the $W_{H\alpha}$ criterion is that the ionized nebulae and the source of ionization have been observed in the same spectrum. Therefore, care is needed when applying it to high-resolution data (e.g. MUSE, Bacon et al., 2010, or SITELLE, Brousseau et al., 2014), where the ionizing source and the nebulae may not be cospatial.

For both CALIFA and MaNGA data (Lacerda et al., 2018; VA19), we have classified spaxels as (a) hDIG ($W_{H\alpha} < 14 \text{ \AA}$), i.e. DIG compatible with ionization by HOLMES; (b) mDIG ($3 < W_{H\alpha} < 14 \text{ \AA}$), for DIG ionized by mixed processes;

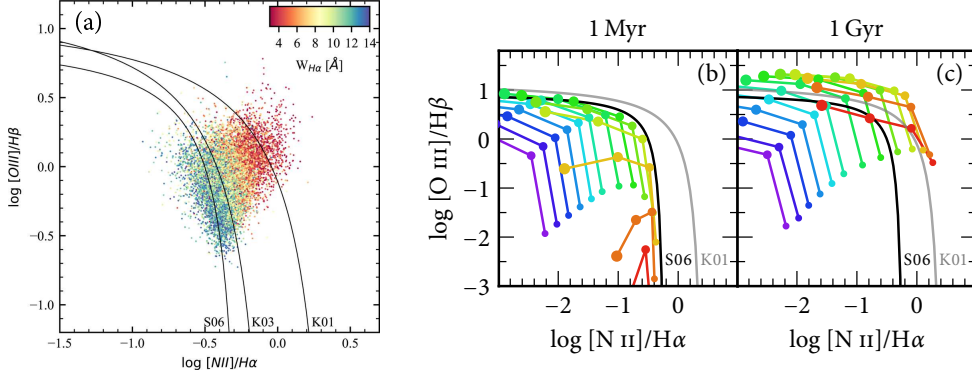


Figure 2. **(a)** Spaxels classified as mDIG from 391 CALIFA galaxies on the $[N\ II]/H\alpha$ versus $[O\ III]/H\beta$ plane, colour-coded by $W_{H\alpha}$. Lines marked as S06, K03 and K01 are the curves by Stasińska et al. (2006); Kauffmann et al. (2003); Kewley et al. (2001). S06 is a line based on photoionization models calibrated on SDSS to the right of which contribution from radiation harder than OB stars is needed to explain the observed emission-line ratios. Regions where $W_{H\alpha}$ is smaller (red points), thus where the contribution of the DIG is larger, have enhanced emission-line ratios. This implies that, the larger the contribution from the DIG, the larger the systematic changes in emission line ratios. **(b)**, **(c)** Photoionization models for $12 + \log O/H = 7.0, 7.2, \dots, 9.4$ (from violet to red) and $\log U = -4, -3, -2, -1$ (from small to big points) for (b) a young SSP, representative of H II regions, and (c) an old SSP, mimicking ionization by HOLMES or another hard source. For the same value of O/H and U , $[N\ II]/H\alpha$ and $[O\ III]/H\beta$ may be enhanced by more than 1.0 dex due to the harder ionizing field. (Panel (a) adapted from figure 9 by Lacerda et al., 2018.)

and (c) SFC ($W_{H\alpha} > 14\ \text{\AA}$), which are dominated by emission from star-forming complexes.

Figure 2 (a) shows spaxels from CALIFA galaxies classified as mDIG in the $[N\ II]/H\alpha$ versus $[O\ III]/H\beta$ plane. Spaxels colour-coded by $W_{H\alpha}$ reveal that, the smaller the $W_{H\alpha}$ value, the more enhanced $[N\ II]/H\alpha$ and $[O\ III]/H\beta$ are. This denotes $W_{H\alpha}$ can be used as a proxy for how much the DIG affects collisional-to-recombination emission line ratios. Panels (b) and (c) of Figure 2 show a sequence of photoionization models run with `cloudy` v. 17.01 (Ferland et al., 2017). Both panels display the same sequence of O/H and ionization parameter (U); panel (b) shows ionization by an 1 Myr (= OB stars) and panel (c) by an 1 Gyr (= HOLMES; but can be viewed as a proxy for a harder ionizing source) simple stellar population (Mollá et al., 2009). This exemplifies how, given a nebula with the same O/H and U , $[N\ II]/H\alpha$ and $[O\ III]/H\beta$ are enhanced if the ionizing field is harder than that of OB stars.

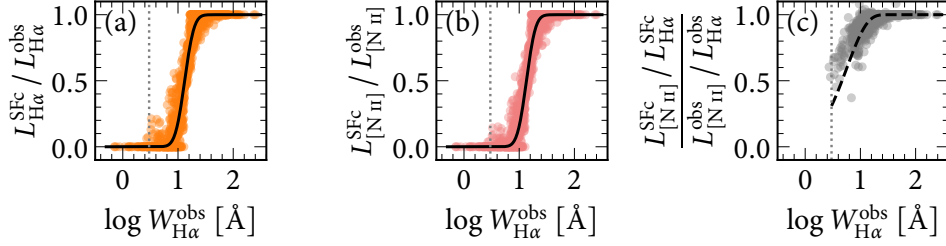


Figure 3. (a) Fraction of $H\alpha$ luminosity in SFC spaxels as a function of the global $W_{H\alpha}$ for 1409 MaNGA galaxies in a circular aperture corresponding to the 0.7 effective radius. The solid line is a fit to the data points, and is suitable to correct fibre-spectroscopy data surveys similar to the SDSS. (b) The same plot for $[N II]$ luminosity. The correction for $[N II]$ is sharper than for $H\alpha$, since the DIG being removed has larger values of $[N II]/H\alpha$. (c) Compound effect of the correction shown in (a) and (b) to the $[N II]/H\alpha$ line ratio (dashed line). Grey points show $[N II]/H\alpha$ for SFC spaxels divided by total $[N II]/H\alpha$. Vertical dotted lines on all panels mark the $W_{H\alpha} > 3 \text{ \AA}$ threshold for which correction is valid. (Panels (a) and (b) adapted from figure 3 by VA19.)

3. Removing the DIG

To correct a given galaxy for the DIG emission, VA19 use the $W_{H\alpha}$ criterion to identify SFC spaxels. Figure 3(a) shows, for 1409 star-forming MaNGA galaxies, the quotient of the $H\alpha$ luminosity due only to SFC spaxels to the total $H\alpha$ luminosity within a 0.7 effective radius. This quotient is plotted as a function of the global $W_{H\alpha}$ of the galaxy: those galaxies with lower global $W_{H\alpha}$ have more spaxels tagged as hDIG or mDIG, so a greater fraction of the $H\alpha$ luminosity is removed when removing DIG spaxels. Figure 3(b) shows the same but for the $[N II]$ luminosity. Crucially, the ‘DIG-correction’ curves for $[N II]$ and $H\alpha$ are slightly different: removing the DIG means removing more light from $[N II]$ than from $H\alpha$. Since the curves in panels (a) and (b) seem almost undistinguishable by eye (but check on table 3 VA19 that they are not exactly the same), panel (c) shows the compound effect of the DIG correction on the $[N II]/H\alpha$ ratio. The y -axis is now the $[N II]/H\alpha$ ratio summing up only SFC spaxels divided by the total $[N II]/H\alpha$ ratio. The dashed line shows the ratio of the curve on panel (b) to the one on panel (a). One can now clearly see how the DIG correction for *line luminosities*, although very similar visually, does imply a change in emission line ratios consistent with the emission line ratio variation due to DIG for individual MaNGA galaxies.

Those DIG-correction curves were calculated for a 0.7 effective radius, which is the typical coverage of galaxies in the fibre-spectroscopic data of the Sloan Digital Sky Survey (SDSS; York et al., 2000). We selected 94 335 star-forming galaxies from the SDSS to check the effect of this correction on O/H and SFR. In the following, we calculate O/H using the $[N II]/H\alpha$ index calibrated by Curti et al. (2017). Results for calibrations based on other emission line indices are shown by VA19.

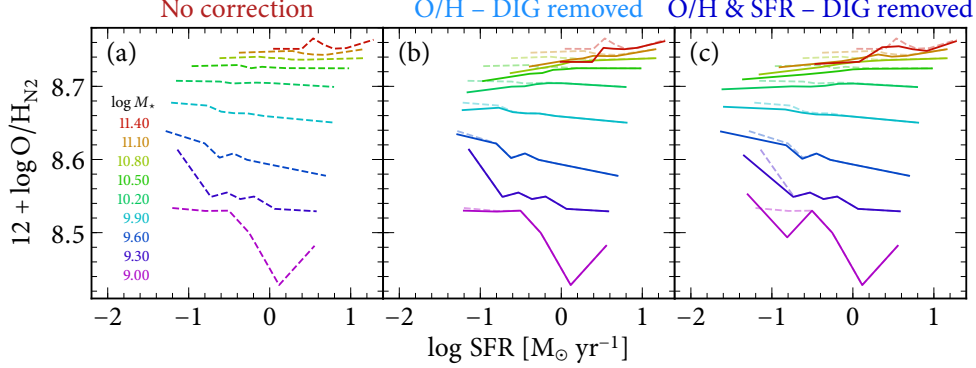


Figure 4. (a) Stellar mass–metallicity–star formation rate relation for 94 335 star-forming SDSS galaxies, where O/H has been estimated from the $[\text{N II}]/\text{H}\alpha$ index. (b) The dashed lines from panel (a) are repeated for comparison. The solid lines show M –O/H–SFR after removing the DIG contribution to $[\text{N II}]$ and $\text{H}\alpha$ prior to computing O/H using the curves from Figure 3. The DIG affects mostly high-mass, low-SFR objects; the flat relations for high-mass bins thus become positive correlations. (c) Similar to panel (b), but after removing the contribution of the DIG for $\text{H}\alpha$ and $\text{H}\beta$ before computing the SFR. The effect of the DIG is small because the correction curves from Figure 3 are based on MaNGA data; at ~ 1 kpc resolution, MaNGA SFC spaxels are still a mix of DIG and H II-region emission. (Figure adapted from figure 5 by VA19.)

Figure 4 compares the mass–metallicity–star formation rate (M –O/H–SFR) relation without any correction, and after removing the DIG contribution. Panel (a) shows the relation with no correction. There is an anti-correlation between O/H and SFR for low- M bins, and no correlation for high- M bins. This result is very similar to the original relation found by Mannucci et al. (2010). Panel (b) repeats the relation in panel (a) in dashed lines, and overplots the new relation after removing the contribution from the DIG to O/H. Galaxies with large M and small SFR are the most affected by the DIG, and so much so that for high- M bins the previously flat correlations become positive correlations. Panel (c) is similar to panel (b), but we have also removed the contribution from the DIG to the $\text{H}\alpha$ and $\text{H}\beta$ luminosities prior to the computation of the SFR.

Those results show that, because strong line methods to measure abundances are calibrated for H II regions, it is dangerous to apply them carelessly when there is an important contribution from the DIG to a galaxy spectrum. The DIG causes O/H values to be systematically overestimated.

We warn that the effect shown here and in VA19 is small because SFC spaxels in MaNGA are not completely devoid of DIG contribution. At the spatial resolution of ~ 1 kpc, they are much larger than classical H II regions. A large sample of higher-resolution spectroscopic data would be needed in order to reveal whether the correction is larger when considering DIG-free H II regions.

Acknowledgments. NVA thanks Grażyna Stasińska and Ariel Werle for suggestions in the manuscript, and acknowledges support of FAPESC, CNPq, and the Royal Society–Newton Advanced Fellowship award (NAF\R1\180403).

References

- Bacon R. et al., 2010, *Ground-based and Airborne Instrumentation for Astronomy III*, Vol. 7735 of *Proc. SPIEJ*, p. 773508
- Blanton M. R. et al., 2017, *AJ*, **154**, 28
- Brousseau D., Thibault S., Fortin-Boivin S., Zhang H., Vallée P., Auger H., Drissen L., 2014, S. K. Ramsay, I. S. McLean, and H. Takami (eds.), *Ground-Based and Airborne Instrumentation for Astronomy V. SPIE*, Vol. 9147 of *Proc. SPIE Conf. Ser.*, p. 91473Z, Bellingham
- Cid Fernandes R., Stasińska G., Mateus A., Vale Asari N., 2011, *MNRAS*, **413**, 1687
- Curti M., Cresci G., Mannucci F., Marconi A., Maiolino R., Esposito S., 2017, *MNRAS*, **465**, 1384
- Dettmar R. J., 1990, *A&A*, **232**, L15
- Ferland G. J., Chatzikos M., Guzmán F., Lykins M. L., van Hoof P. A. M., Williams R. J. R., Abel N. P., Badnell N. R., Keenan F. P., Porter R. L., Stancil P. C., 2017, *RevMexAA*, **53**, 385
- Flores-Fajardo N., Morisset C., Stasińska G., Binette L., 2011, *MNRAS*, **415**, 2182
- Gomes J. M. et al., 2016, *A&A*, **588**, A68
- Haffner L. M., Dettmar R.-J., Beckman J. E., Wood K., Slavin J. D., Giammanco C., Madsen G. J., Zurita A., Reynolds R. J., 2009, *Reviews of Modern Physics*, **81**, 969
- Hoyle F., Ellis G. R. A., 1963, *Australian Journal of Physics*, **16**, 1
- Kaplan K. F., Jogee S., Kewley L., Blanc G. A., Weinzirl T., Song M., Drory N., Luo R., van den Bosch R. C. E., 2016, *MNRAS*, **462**, 1642
- Kauffmann G. et al., 2003, *MNRAS*, **346**, 1055
- Kewley L. J., Dopita M. A., Sutherland R. S., Heisler C. A., Trevena J., 2001, *ApJ*, **556**, 121
- Lacerda E. A. D., Cid Fernandes R., Couto G. S., Stasińska G., García-Benito R., Vale Asari N., Pérez E., González Delgado R. M., Sánchez S. F., de Amorim A. L., 2018, *MNRAS*, **474**, 3727
- Mannucci F., Cresci G., Maiolino R., Marconi A., Gnerucci A., 2010, *MNRAS*, **408**, 2115
- Mollá M., García-Vargas M. L., Bressan A., 2009, *MNRAS*, **398**, 451
- Sánchez S. F. et al., 2016, *A&A*, **594**, A36
- Stasińska G., Cid Fernandes R., Mateus A., Sodr  L., Asari N. V., 2006, *MNRAS*, **371**, 972
- Stasińska G., Vale Asari N., Cid Fernandes R., Gomes J. M., Schlickmann M., Mateus A., Schoenell W., Sodr  Jr. L., 2008, *MNRAS*, **391**, L29
- Vale Asari N., Couto G. S., Cid Fernandes R., Stasińska G., de Amorim A. L., Ruschel-Dutra D., Werle A., Florido T. Z., 2019, *MNRAS*, **489**(4), 4721
- York D. G. et al., 2000, *AJ*, **120**, 1579
- Zhang K. et al., 2017, *MNRAS*, **466**, 3217